Modeling of an Electric Vehicle Charging Station for Fast DC Charging

Arnaldo Arancibia
School of Electrical Engineering and Computer Science
Technical University of Berlin
10587 Berlin, Germany
Email: arnaldo.arancibia@mailbox.tu-berlin.de

Kai Strunz
School of Electrical Engineering and Computer Science
Technical University of Berlin
10587 Berlin, Germany
Email: kai.strunz@tu-berlin.de

***Abstract*—The proposed model of an electric vehicle charging station is suitable for the fast DC charging of multiple electric vehicles. The station consists of a single grid-connected inverter with a DC bus where the electric vehicles are connected. The control of the individual electric vehicle charging processes is decentralized, while a separate central control deals with the power transfer from the AC grid to the DC bus. The electric power exchange does not rely on communication links between the station and vehicles, and a smooth transition to vehicle-to-grid mode is also possible. Design guidelines and modeling are explained in an educational way to support implementation in Matlab/Simulink. Simulations are performed in Matlab/Simulink to illustrate the behavior of the station. The results show the feasibility of the model proposed and the capability of the control system for fast DC charging and also vehicle-to-grid.**

I. Introduction

Charging time reduction is one of the key goals in making electric vehicles user-friendly. In this context, fast DC charging offers an interesting opportunity. It allows for reducing charging times to ranges of 10 to 20 minutes [1]. The SAE J1772 standard defines three levels of fast DC charging as DC Level 1 200/450 V, up to 36 kW (80 A); DC Level 2 - 200/450 V, up to 90 kW (200 A) and DC Level 3 200/600 V DC (proposed) up to 240 kW (400 A) [1]. All levels use off-board electric vehicle supply equipment (EVSE).

In this paper, modeling and simulation of an electric vehicle charging station for fast DC charging are proposed and formulated in an educational way in order to allow its implementation and further research on the topic.

In the following sections, important aspects of an EV charging station model are developed. In Section II, the design of the circuit is considered. Control methods for DC charging of EVs and the charging station are considered in Section III. In Section IV, simulations substantiate the made claims and illustrate the operation of the proposed charging station. Finally, conclusions are presented in Section V.

II. Charging Station Design

A variety of aspects needs to be taken into account when designing the circuit of the charging station. These aspects, from a technical point of view, include the following:

- Area made available for parking of vehicles; this influences the number of cars that can be placed and charged.
- Estimation of the demand for fast charging slots in the location.
- Network parameters, i.e. nominal voltage and allowable power levels at the point of common coupling (PCC).
- Maximum charging power rate for individual vehicles.

The proposed DC charging station configuration is shown in Fig. 1, it can be seen that the inverter is interfaced to the network through an LCL filter and a transformer; while a single DC bus feeds all individuals battery chargers.

The charging station rated capacity S_{rated} in VAr is defined according to (1):

$$S_{\mathrm{rated}} = \frac{k_{\mathrm{load}} N_{\mathrm{slot}} P_{\mathrm{EV}}}{\cos\phi} \tag{1}$$

where $\cos\phi$ is the power factor, N_{slot} is the amount of charging slots available for individual EVs, P_{EV} is the maximal power rate of an individual EV and k_{load} is an overload factor for cover overloading in transients.

Generally, the DC link voltage is set according to the grid voltage. In this work, the grid connection through a transformer leaves the DC bus voltage selection free from the grid voltage level. However, it has to be considered that the battery minimum voltage $V_{\mathrm{bat}}^{\mathrm{min}}$, and the battery charger minimum modulation index m_{min}, define an upper bound for the DC bus voltage as in (2):

$$v_{\mathrm{dc}} \leq \frac{V_{\mathrm{bat}}^{\mathrm{min}}}{m_{\mathrm{min}}} \tag{2}$$

where v_{dc} is the DC bus nominal voltage.

A. DC bus capacitance calculation

The stability of the DC bus depends directly on the DC capacitance size. Basically, it has to support the DC current ripple. As many EV chargers can be connected to the DC bus, ripple current can be very high needing for a huge capacitance. A good method to define the capacitance of a DC bus, including the resistance and the inductance of the cable is reported in [2]. Additionally, a practical method is reported in [3]. In this work, both methods are taken into account, and the DC capacitance is determined by the capacitor energy rate of change during transients and the rated active power. The calculation is proposed in (3):

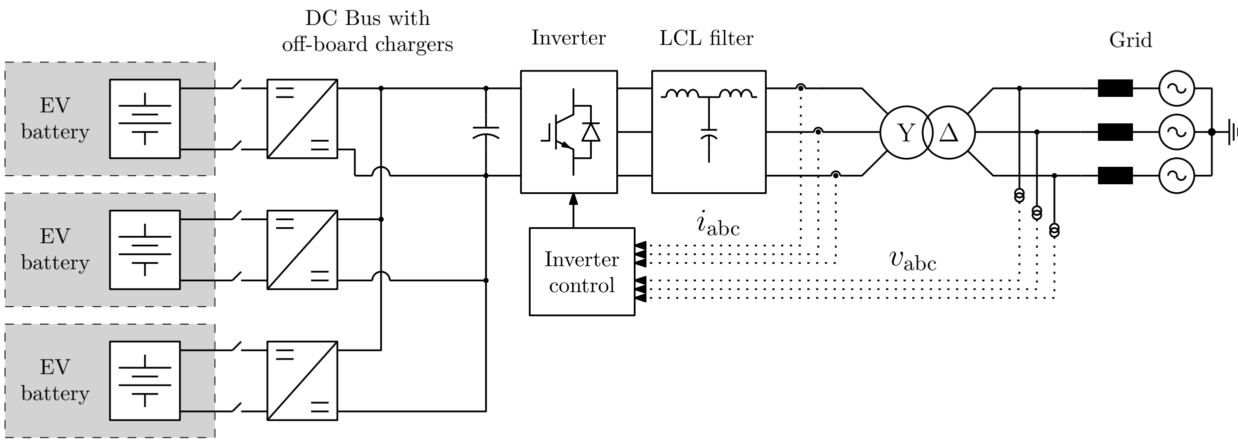

Fig. 1. Proposed EV charging station for fast DC charging.

$$C_{\mathrm{dc}} = \frac{S_{\mathrm{rated}}}{V_{\mathrm{dc}}^2} \frac{2nT\Delta r \cos\phi}{\Delta x} \tag{3}$$

where T is the period of the AC voltage waveform, n is a multiple of T, Δr is the DC power range of change, in percent, during transients, and Δx is the allowable DC bus voltage range of change, in percent, during transients.

B. EV battery

Nowadays, run time based models combined with Thévenin equivalent based models are the state of the art [4]. In this work, such an approach is used. Fig. 2 shows the electric circuit configuration of the battery model. Here V_{oc} is the open circuit voltage which is depending of the state of charge SOC, and the voltage-current characteristic is modeled by a series resistance R_{series}. The RC parallel circuit represents the transient response of the battery.

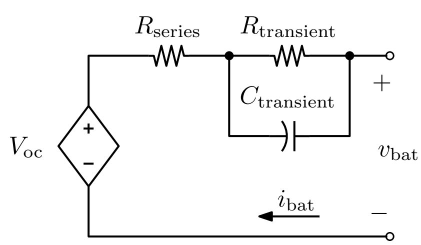

Fig. 2. Thévenin battery model.

C. Battery charger

Fig. 3 shows the modeled battery charger. It consists of a bi-directional DC-DC converter with two IGBT switches that are operated always by complimentary control signals [5]. This allows a continuous bi-directional power capability. When the lower switch is operating, the converter boosts the left-side voltage v_{bat}, and the current i_{bat} in the inductor L_{bat} flows to the capacitor C. When the upper switch is operating, the converter acts as buck-type converter, and i_{bat} flows from capacitor C to the inductor obtaining an opposite direction of i_{bat}.

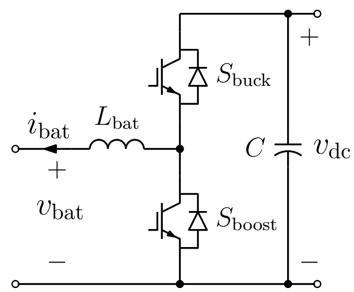

Fig. 3. Battery charger configuration.

D. Three-phase inverter

In this work for an educational purpose and simplicity of modeling, the inverter configuration is chosen as in Fig. 4. Here, the inverter is connected to an LCL filter.

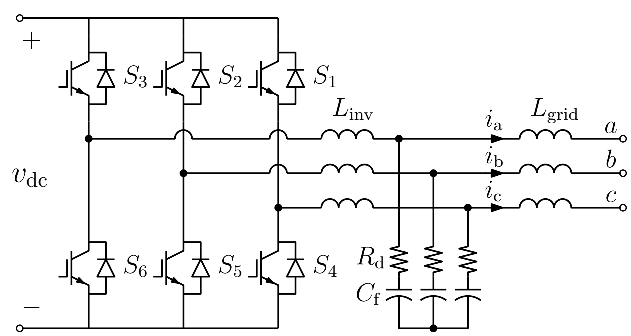

Fig. 4. Three-phase inverter plus LCL filter.

E. LCL filter

Passive LCL filters become as state of the art in harmonic reduction of grid-interfaced distributed power sources [6]. Different methodologies to determine the filter parameters can be found in the literature [7]–[9].

On the one hand, the selection of the inverter side inductance is based on DC voltage, inverter modulation index, switching frequency and current total harmonic distortion

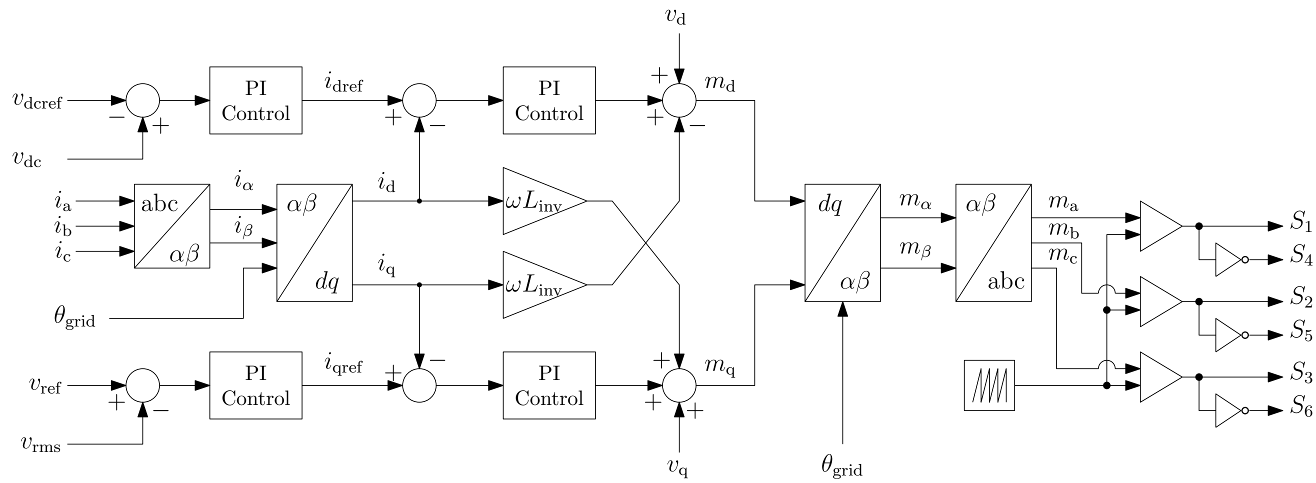

Fig. 5. Charging station control system.

THD. On the other hand, the selection of capacitance, and grid-side inductance depends on the grid parameters, reactive power, resonance frequency, and ripple attenuation factor (RAF) [7].

Fig. 4 shows the LCL filter configuration where the inverter-side inductance L_{inv}, filter capacitance C_{f} and grid side inductance L_{grid} are determined as in (4), (5), (6) respectively:

$$L_{\mathrm{inv}} = \frac{V_{\mathrm{grid}}^2}{S_{\mathrm{rated}} \cdot THD \cdot 2\pi f_{\mathrm{sw}}} \sqrt{\frac{\pi^2}{18}\left(\frac{3}{2} - \frac{4\sqrt{3}}{\pi} m_{\mathrm{a}} + \frac{9}{8} m_{\mathrm{a}}^2\right)} \tag{4}$$

$$C_{\mathrm{f}} \leq \frac{0.05 S_{\mathrm{rated}}}{2\pi \cdot f_{\mathrm{grid}} \cdot V_{\mathrm{grid}}^2} \tag{5}$$

$$L_{\mathrm{grid}} = \frac{RAF + 1}{RAF \cdot C_{\mathrm{f}} \cdot 2\pi f_{\mathrm{sw}}^2} \tag{6}$$

In the previous equations, f_{sw} is the switching frequency of the inverter, f_{grid} is the grid voltage fundamental frequency, m_{a} is the inverter modulation index. THD is normally set between 5% and 30% [8] and RAF normally around 20% [7].

After obtaining the filter parameters, it should be verifiable that resonance frequency, defined in (7), should be in the range of less than half of the f_{sw} and 10 times bigger than the grid frequency [7].

$$\omega_{\mathrm{res}} = \sqrt{\frac{L_{\mathrm{inv}} + L_{\mathrm{grid}}}{L_{\mathrm{grid}} L_{\mathrm{inv}} C_{\mathrm{f}}}} \tag{7}$$

If the resultant parameters do not match this condition, determination of C_{f}, range of THD and range of RAF gives flexibility to match this condition. Finally, a damping resistor R_{d} is included as shown in Fig. 4 and it is calculated as in (8):

$$R_{\mathrm{d}} = \frac{1}{3 C_{\mathrm{f}} \omega_{\mathrm{res}}} \tag{8}$$

III. CONTROL SYSTEM

On the one hand, the inverter deals with the power exchange between the AC grid and the DC bus. Simultaneous EV charging and a smooth transition to vehicle-to-grid (V2G) mode is also possible. This control does not rely on communication links between the inverter and individual EVs. On the other hand, the control of the individual EV depends on battery state of charge SOC and the current i_{bat}.

A. Inverter control

A cascade control in the dq-frame is proposed. It consists of outer voltage loop and inner current loop [10], [11]. Synchronization with the grid voltage is performed through a phase locked loop (PLL) [12]. The proposed control methodology is depicted in Fig. 5. The d-axis outer loop controls the DC bus voltage, and the inner loop controls the active AC current. Because the inverter allows bidirectional power flow, increments in the DC bus voltage can be produced from negative or positive current direction and vice versa. The q-axis outer loop regulates the AC voltage magnitude by adjusting the reactive current, which is controlled by the q-axis inner current loop. Additionally, dq decoupling-terms ωL_{inv} and feed-forward voltage signals are added to improve the performance during transients.

Fig. 6 shows the PLL block diagram where the input is the measured three-phase voltage at PCC. The output signals v_{d}, θ_{grid}, and ω are obtained to use in the dq-frame inverter control.

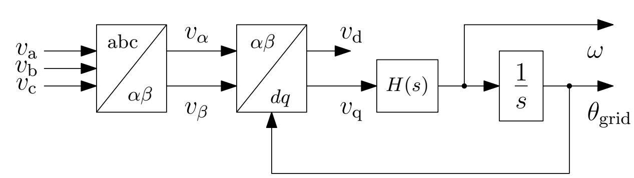

Fig. 6. Charging station PLL block diagram.

B. Battery charger control

Two equivalent control methodologies can be implemented depending on desired charging strategy: constant current and constant voltage.

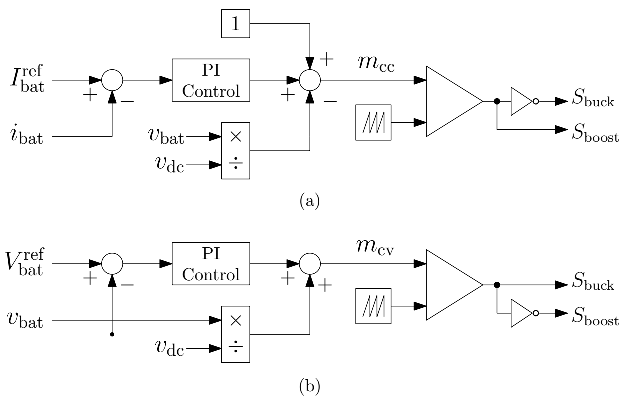

Fig. 7. Battery charger control: (a) constant current strategy, (b) constant voltage strategy.

1) Constant current strategy: It is a unified control strategy equivalent to operating the battery as a current source. The output duty ratio m_{cc} defines the boost-mode operation of the converter. This strategy is depicted in Fig. 7(a).

2) Constant voltage strategy: Analog to the constant current strategy, constant voltage strategy is equivalent to operating the battery as voltage source. The output duty ratio m_{cv} defines the buck-mode operation of the converter. This strategy is depicted in Fig. 7(b).

IV. Simulation Results

Considering the design procedure of the previous Sections, an example model is implemented in Matlab/Simulink SimPowerSystem. Table I gives the input parameters, while Table II gives the resulting parameters of the model.

The battery model can be implemented as depicted in Fig. 2 or, alternatively, to use the "battery" block provided in the SimPowerSystems Library [13]. The battery charger can be implemented with parameters from Table II and Fig. 3. The inverter can be implemented with the block "universal bridge" from the SimPowerSystems Library. It has to be selected "3 arms" and $R_{\text{on}} = 0.01\,\Omega$. The transformer can be implemented directly with the "three-phase two windings transformer" block. Finally, the AC source can be implemented with the block "Three-phase source" and the parameters from Table I. The complete model implemented in MATLAB/Simulink SimPowerSystems is depicted in Fig. 8, where only two EVs appear as example.

Before running the simulation, it is important to set an appropriate simulation time step and an integration method. To achieve good results, the integration method should have at least 100 sample points in a period of the fastest frequency [14]. In the example model, the fastest frequency is $f_{\text{sw}} = 5000$ Hz. The selected integration method is ode23t, and the simulation time step is set as in (9):

TABLE I
CHARGING STATION INPUT PARAMETERS

Parameters	Values
N_{slot}	10
EV charging current	200 A
P_{EV}	90 kW
$\cos\phi$	0.95
k_{load}	1.1
V_{bat}^{min}	200 V
m_{min}	0.125
L_{bat}	2 mH
R_{series}	0.0175 Ω
$R_{\text{transient}}$	0.245 Ω
$C_{\text{transient}}$	8100 mF
V_{oc}	400 V
Battery capacity	35 kWh
Battery time constant	2 s
SOC	50 %
T	1/50 s
n	0.5
f_{sw}	5000 Hz
V_{grid}	20 kV ph-ph
f_{grid}	50 Hz
short circuit level	1200 MVA
X/R ratio	8

TABLE II
CHARGING STATION RESULTING PARAMETERS

Parameters	Values
S_{rated}	1050 kVA
V_{dc}	1.5 kV
Δx	20%
Δr	10%
C_{dc}	18 mF
Transformer	20/0.8 kV Δ-Y_{g}
L_{inv}	0.48 mH
L_{grid}	0.69 mH
C_{f}	165 μF
R_{d}	1.31 Ω

$$\tau_{\text{s}} = \frac{1\ \text{s}}{5000 \times 100} = 2\ \mu\text{s} \tag{9}$$

A. Performance to load changes

Fig. 9 shows the results of the charging station for a simultaneous connection of two EVs. At $t = 0$ s, the charging station is operating at no load. At $t = 0.2$ s, two EVs are simultaneously connected and charged at maximum power as Fig. 9(a) shows. It can be seen that Q is almost not affected by the load change of P from 0 kW to -180 kW. Fig. 9(b) shows the response of the DC bus voltage to this load change. Here, the variation of the voltage is less than 25 V, and it is stabilized in less than 0.1 s.

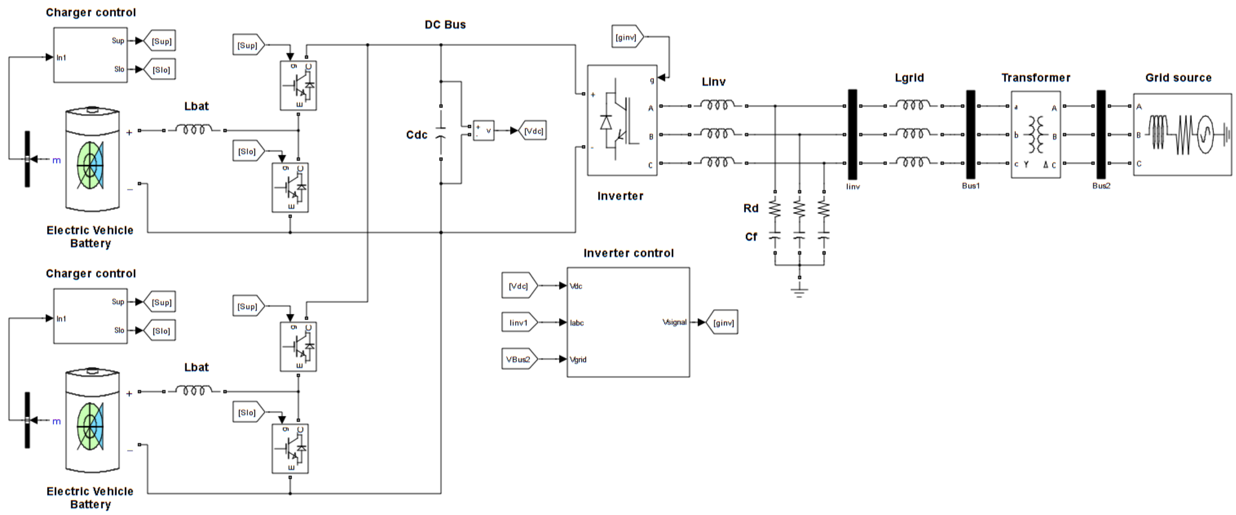

Fig. 8. Matlab/Simulink SimPowerSystems implementation of the EV charging station.

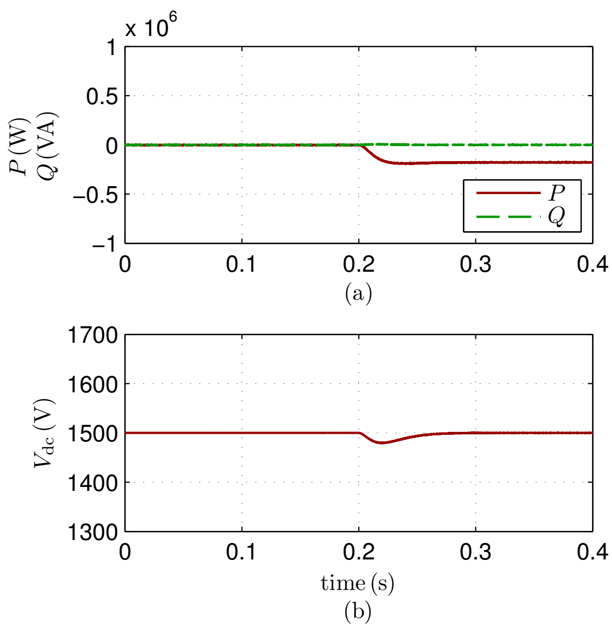

Fig. 9. Charging station results for two EVs load change: (a) active and reactive power, (b) DC bus voltage.

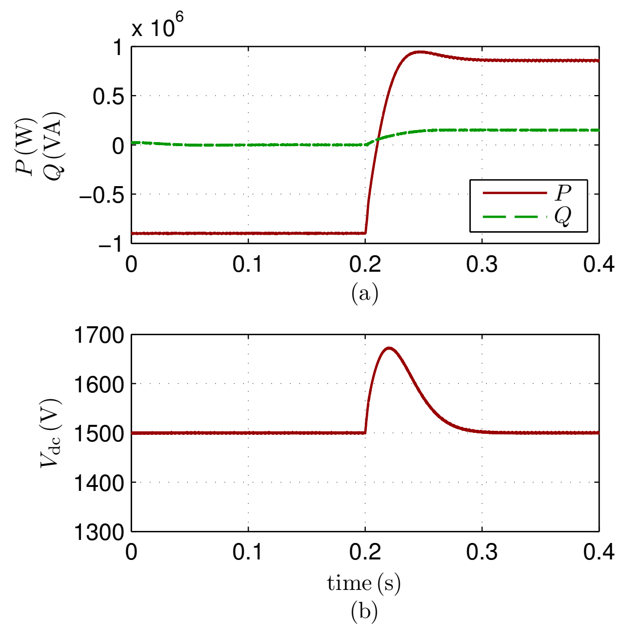

Fig. 10. Charging station results for V2G and reactive power compensation: (a) active and reactive power, (b) DC bus voltage.

B. V2G capability and reactive power compensation

Fig. 10 shows the results of the charging station performing V2G and reactive power compensation. Fig. 10(a) shows that at $t = 0$ s, the charging station is operating at $P = -900$ kW and $Q = 0$ kVAr. At $t = 0.2$ s, V2G at maximum available power and an injection of 150 kVAr are required. Fig. 10(b) shows the response of the DC bus voltage to V2G and reactive power compensation. The change in the current direction influences a positive voltage variation, as it is expected. These results are according to the design parameters for the DC bus capacitance. In addition, reactive power compensation does not affect considerably the dynamics of the DC bus voltage.

C. Charging and discharging of an EV battery

Fig. 11 shows the results for an EV battery during charging and discharging. The control methodology implemented is constant current. When the battery is charging at constant current, the voltage is higher than its open circuit value as Fig. 11(a) and Fig. 11(b) show, respectively. At $t = 0.2$ s, the battery is discharged at constant current and the voltage decreases as Fig. 11(a) and Fig. 11(b) demonstrate, respectively. From these results, it can be noticed that, due to the voltage difference, EV charging and V2G have different power rates for the same current.

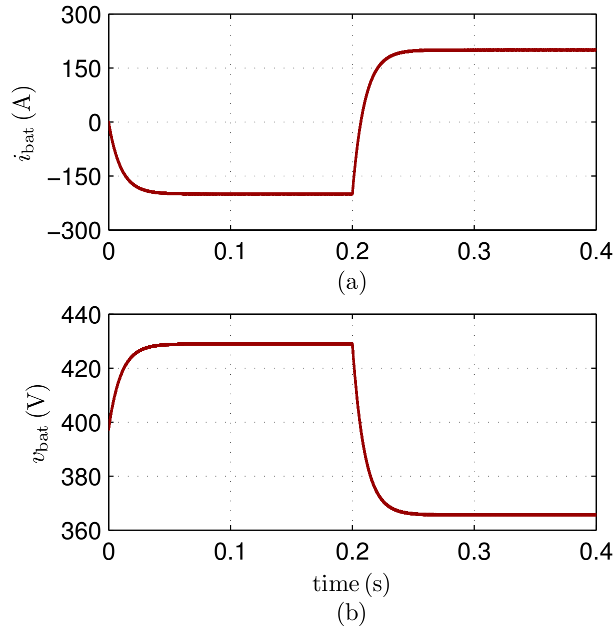

Fig. 11. Individual EV battery results for charging and discharging: (a) battery voltage, (b) battery current.

V. Conclusions

A new model of a charging station for fast DC charging is presented. The modeling of every component is presented with their corresponding parameters. In addition, a control system is also included. The modeling procedure is explained in an educational manner in order to allow further research on the topic. The practical implementation of the model in MATLAB/Simulink SimPowerSystems is also described, considering simulation aspects, as the time step and the integration method. The charging station model was also designed to support V2G and reactive power compensation. A one megawatt rated charging station, with ten EVs capacity, is simulated with realistic parameters. It was found that DC fast charging of multiple EVs is possible. Simulation results show a proper dynamic behavior of the DC bus voltage, the battery voltage, and the battery current. Moreover, the results show that a smooth transition to V2G and reactive power compensation are possible.

References

[1] http://www.sae.org/smartgrid/chargingspeeds.pdf
[2] Karlsson, P. Svensson, J. , "DC bus voltage control for a distributed power system," Power Electronics, IEEE Transactions on , vol.18, no.6, pp. 1405- 1412, Nov. 2003.
[3] Mishra, M.K. Karthikeyan, K. , "A Fast-Acting DC-Link Voltage Controller for Three-Phase DSTATCOM to Compensate AC and DC Loads," Power Delivery, IEEE Transactions on , vol.24, no.4, pp.2291-2299, Oct. 2009.
[4] Min Chen and Rincon-Mora, G.A., "Accurate electrical battery model capable of predicting runtime and I-V performance" IEEE Transactions on Energy Conversion, VOL. 21, NO. 2, June 2006.
[5] Mohan, N. "First Course on Power Electronics Converters and Drives" Minneapolis, USA. ISBN 0-9715292-2-1.
[6] Dannehl, J. Fuchs, F.W. Thgersen, P.B. , "PI State Space Current Control of Grid-Connected PWM Converters With LCL Filters," Power Electronics, IEEE Transactions on , vol.25, no.9, pp.2320-2330, Sept. 2010.
[7] Min-Young Park, Min-Hun Chi, Jong-Hyoung Park, Heung-Geun Kim, Tae-Won Chun, Em-Cheol Nho, "LCL-filter design for grid-connected PCS using total harmonic distortion and ripple attenuation factor," Power Electronics Conference (IPEC), 2010 International , vol., no., pp.1688-1694, 21-24 June 2010.
[8] Araujo, S.V. Engler, A. Sahan, B. Antunes, F., "LCL filter design for grid-connected NPC inverters in offshore wind turbines," Power Electronics, 2007. ICPE '07. 7th Internatonal Conference on , vol., no., pp.1133-1138, 22-26 Oct. 2007.
[9] M. Tavakolini Bina, E. Pashajavid "An efficient procedure to design passive LCL-filters for active power filters"'. Electric System Power Research. 2009.
[10] Yazdani, A. Iravani, R. "Voltage-Sourced Converters in Power Systems - Modeling, Control and Applications" John Wiley and Sons, 2009 - Technology and Engineering.
[11] Blaabjerg, F. Teodorescu, R. Liserre, M. Timbus, A.V., "Overview of Control and Grid Synchronization for Distributed Power Generation Systems," Industrial Electronics, IEEE Transactions on , vol.53, no.5, pp.1398-1409, Oct. 2006.
[12] Se-Kyo Chung, "A phase tracking system for three phase utility interface inverters ," Power Electronics, IEEE Transactions on , vol.15, no.3, pp.431-438, May 2000.
[13] MATLAB Simulink SimPowerSystems 7.6 (R2008a) "SimPowerSystems Library Documentation" 2008.
[14] Mohan, N. Undeland, T. Robbins, W. "Power Electronics Converters, Applications, and Design" ISBN 0-471-22693-9.